Radiation families emitted by a discrete soliton in parity-time-symmetric waveguide arrays

Anuj P. Lara ●,[1] Ambaresh Sahoo,[2,3] and Samudra Roy[1,*]

[1]*Department of Physics, Indian Institute of Technology Kharagpur, Kharagpur 721302, India*
[2]*Department of Physical and Chemical Sciences, University of L'Aquila, Via Vetoio, L'Aquila 67100, Italy*
[3]*Department of Physics, Harimohan Ghose College, Kolkata 700024, India*

We investigate the dynamics of a spatial discrete soliton and the radiation families emitted by it inside a parity-time ($\mathcal{PT}$)-symmetric waveguide array with alternate gain-loss channels. A strong spatial soliton that evolves inside the waveguide array due to the balance between discrete diffraction and Kerr nonlinearity excites linear waves in the form of diffractive radiation when launched with an angle. The $\mathcal{PT}$-symmetric nature of the waveguide leads to additional radiations in Fourier space that have not been explored. In our paper, we mainly focus on the origin of these radiations and try to understand how to control them. Under strong $\mathcal{PT}$ symmetry, a discrete soliton launched normally to the waveguide array produces strong side lobes, which can lead to a population of the field at $\pm\pi/2$ in momentum space. In addition, a strong soliton with initial phase gradient radiates a unique $\mathcal{PT}$-symmetry-assisted linear wave. We establish a phase-matching condition to locate such radiation in momentum space. The periodic arrangement of the gain-loss channel also leads to radiations due to reflection and backscattering, which is prominent for a weak soliton. A linear Hamiltonian analysis for such a waveguide array is provided to identify the $\mathcal{PT}$-phase-transition regime and to optimize the parameters for stable discrete soliton dynamics. We thoroughly investigate the origin of all the radiations that emerge in the $\mathcal{PT}$-symmetric waveguide array and put forward the background theory, which is in good agreement with the full numerical results.

I. INTRODUCTION

A linear waveguide array (WA) is a periodic photonic structure where a propagating optical wave experiencing spatially periodic refractive index distribution behaves like an electron traveling through a semiconductor crystal. The one-dimensional homogeneous WAs that are evanescently coupled to each other allow the light beam to propagate in a transverse direction, resulting in a phenomenon called *discrete diffraction*. The optical Kerr nonlinearity counterbalances the discrete diffraction and exhibits localized structure in the form of a *discrete soliton* (DS). The dynamics of the DS is governed by the discrete nonlinear Schrödinger equation (DNLSE). These spatially localized structures manifest properties that are intriguing and forbidden in the case of their continuous counterparts. A few examples are Anderson localization [1,2], photonic Bloch oscillations, localized Wannier-Stark states [3,4], and Bloch-Zener oscillation and photonic Zener tunneling [5,6].

Diffractive resonant radiation (DifRR), which is the spatial or (wave-number) analog of the dispersive resonant radiation in the time (frequency) domain, has primarily been investigated in uniform WAs supporting DSs as a theoretical perspective [7]. This concept is further extended in supercontinuum generation in both frequency and wave-number domains [8]. Unlike temporal dispersive radiations, which are controlled by zero-dispersion wavelengths and span any frequency range [9], the DifRR is strictly confined within the first Brillouin boundary ($\pm\pi$) in wave-number space. Any electric field that encounters this Brillouin boundary results in 2π phase shift and appears from the opposite wave-number boundary, a phenomenon termed as *anomalous recoil* [7]. In uniform WAs, the generation of DifRR requires an initial nonzero wave number of the DS, while its manipulation and control can be achieved through the soliton power and coupling. However, with the introduction of chirp in WAs [10], there is an additional degree of freedom (chirp) other than the wave number that tailors the generation of DifRR. In this scheme, it is even possible to generate dual DifRR with the introduction of a symmetrically chirped WA.

Moving forward with the WAs, in recent years, the non-Hermitian Hamiltonian with $\mathcal{PT}$ symmetry or broadly speaking non-Hermitian quantum physics has emerged as a fascinating topic in both theoretical and experimental physics after Bender and Boettcher put forward the mathematical idea in 1998 [11]. A non-Hermitian Hamiltonian $\hat{H}$ is considered to be $\mathcal{PT}$ symmetric if $[\hat{H}, \mathcal{PT}] = 0$, where $\mathcal{P}$ and $\mathcal{T}$ respectively denote the parity (space reflection) and time-reversal ($i = \sqrt{-1}$ flips sign) operators. One notable aspect of such Hamiltonians is the breaking of $\mathcal{PT}$ symmetry, in which the eigenspectra transition from completely real (unbroken $\mathcal{PT}$ regime) to complex values (broken $\mathcal{PT}$ regime) across a $\mathcal{PT}$-phase-transition point called the *exceptional point* (EP), where at least two eigenvalues and corresponding eigenvectors coalesce and become degenerate [12,13]. The concept of $\mathcal{PT}$ symmetry is most appreciated in the field of optics, which offers a suitable platform to practically demonstrate unique non-Hermitian features such as unidirectional light propagation or optical nonreciprocity [14], loss-induced transparency

*samudra.roy@phy.iitkgp.ac.in

[15], optical solitons [16], and enhanced light-matter interactions [17,18].

$\mathcal{PT}$-symmetric WAs with balanced loss-gain offer new possibilities in shaping light beams, which have been used in various contexts [19–21]. In this paper, we explore the generation of different kinds of radiations in momentum space (k space) of WAs with alternate gain and loss channels supporting DSs. With the introduction of $\mathcal{PT}$-symmetric WAs, we observe two families of radiation assisted solely by the $\mathcal{PT}$ symmetry. The locations of these radiations can be controlled further by changing the gain-loss coefficient that opens up possibilities in designing novel photonic devices and controlling the flow of light at the nanoscale level.

We organize the paper as follows. In Sec. II, we describe the setup and establish the governing equation for a discrete soliton excited in a $\mathcal{PT}$-symmetric WA. We also provide a background theory of DifRR and develop a linear Hamiltonian analysis for $\mathcal{N}$-channel $\mathcal{PT}$-symmetric WA. In Sec. III, we carefully analyze different radiations emitted by the DS in k space due to the $\mathcal{PT}$-symmetric nature of the WA. Finally, in Sec. IV we summarize our results and conclude.

II. SYSTEM SETUP AND THEORETICAL FRAMEWORK

In our investigation, we consider a $\mathcal{PT}$-symmetric WA that consists of alternative gain-loss channels having a neutral waveguide at the center ($n = 0$). This neutral waveguide acts like a defect. The proposed waveguide array is schematically shown in Fig. 1(a). We use a minimalistic and simple design here by keeping the spacing between two adjacent waveguides constant over the entire array. Assuming that the couplings between gain-loss, gain-neutral, and neutral-loss channels are all identical, the mode evolution in the nth waveguide E_n can be described by the following normalized equation:

$$i\frac{d\psi_n}{d\xi} + c[\psi_{n+1} + \psi_{n-1}] + |\psi_n|^2\psi_n = \text{sgn}(n)(-1)^n i\Gamma\psi_n,$$

(1)

where $\psi_n = E_n/\sqrt{P_0}$, with P_0 being the peak power of the input field. Range of the index n is considered within $-N \leqslant n \leqslant N$, thereby defining the total number of waveguides to be $\mathcal{N} = (2N + 1)$. The propagation distance (z) and coupling coefficient (C) between adjacent waveguides are rescaled as $\xi \to z/L_{\text{NL}}$ and $c \to CL_{\text{NL}}$, where nonlinear length is defined by $L_{\text{NL}} = (P_0\gamma)^{-1}$ and γ is the nonlinear parameter in units of $\text{W}^{-1}\text{m}^{-1}$. The gain-loss parameter g having the unit of m^{-1} is rescaled as $\Gamma = gL_{\text{NL}}$. The axis ξ, along with the parameters c and Γ, are therefore normalized and dimensionless. Since this paper aims to investigate the formation and control of DifRRs in $\mathcal{PT}$-symmetric WAs, first we study the dynamics of DSs in the simplest $\mathcal{PT}$-symmetric WAs as described in Fig. 1(a). We
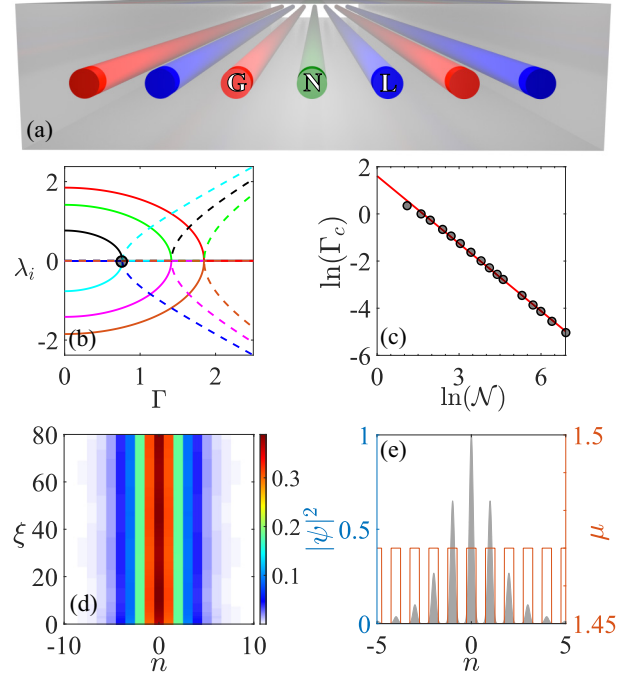

FIG. 1. (a) Schematic diagram of the $\mathcal{PT}$-symmetric waveguide array consisting of alternative gain and loss channels with a neutral central waveguide. (b) The variation of real (solid) and imaginary (dotted) components of the eigenvalues of a seven channel $\mathcal{PT}$-symmetric WA as a function of Γ. Here, the circle represents the exceptional point (Γ_c). (c) Variation of the critical point (exceptional point) Γ_c as a function of the total number of waveguides $\mathcal{N}$ (in natural log scale). (d) A discrete soliton in a waveguide array, with (e) the mode distribution along with the refractive index profile.

excite DSs in the unbroken $\mathcal{PT}$ regime since the broken $\mathcal{PT}$ regime causes instability [16]. To identify the unbroken $\mathcal{PT}$ regime, we implement a Hamiltonian analysis and determine the parameter space (relation between the coupling and gain-loss coefficients) for stable DS excitation.

A. Hamiltonian analysis

The dynamics of the electric field inside the $\mathcal{N}$-channel $\mathcal{PT}$-symmetric WA with central defect as neutral channel [see Fig. 1(a)] is modeled by Eq. (1). This governing equation [Eq. (1)] can be rearranged in a matrix form [22], $id_\xi\Psi = \hat{H}\Psi$, where $\Psi = [\psi_{-N}; \psi_{-(N-1)}; \ldots; \psi_{-1}; \psi_0; \psi_1; \ldots; \psi_{(N-1)}; \psi_N]$ is the column vector formed by the $\mathcal{N}$ elements in the array. The $\mathcal{PT}$-symmetric Hamiltonian $\hat{H}$ for such system which satisfies $[\hat{H}, \mathcal{PT}] = 0$ can be constructed with unitary coupling ($c = 1$) and balanced gain and loss Γ as

$$\hat{H} \equiv \begin{bmatrix} -(-1)^N i\Gamma & -1 & 0 & . & . & . & 0 \\ . & . & . & . & . & . & . \\ 0 & . & i\Gamma & -1 & 0 & . & 0 \\ 0 & . & -1 & 0 & -1 & . & 0 \\ 0 & . & 0 & -1 & -i\Gamma & . & 0 \\ . & . & . & . & . & . & . \\ 0 & . & . & . & 0 & -1 & (-1)^N i\Gamma \end{bmatrix}_{\mathcal{N}\times\mathcal{N}}.$$

(2)

The $\mathcal{N}$ eigenvalues of the system can be obtained by diagonalizing the Hamiltonian matrix. Considering a three-channel gain-neutral-loss waveguides system for simplicity, the $[3{\times}3]$ Hamiltonian can be written as $\hat{H}_3 \equiv [i\Gamma, -1, 0; -1, 0, -1; 0, -1, -i\Gamma]$, which results in the eigenvalues 0 and $\pm\sqrt{2-\Gamma^2}$. Here, $\Gamma = \Gamma_c = \sqrt{2}$ acts as the critical value at which the eigenvalues transit from real to imaginary with the real components collapsing to zero at this point [18,22]. This critical point is termed as the *exceptional point*, where the $\mathcal{PT}$ symmetry breaking takes place (a third-order EP in this case). For a higher number of waveguide channels, the eigenvalues take more complex forms and need to be evaluated numerically. Such a set of eigenvalues is obtained numerically for a system of seven channels and plotted in Fig. 1(b). Note, that the lowest value of Γ_c depends on the number of waveguide channels. To establish the empirical relation between waveguide channel ($\mathcal{N}$) and Γ_c we numerically calculate the set of eigenvalues from the $[\mathcal{N}{\times}\mathcal{N}]$ Hamiltonian as given in Eq. (2). In Fig. 1(c), we plot Γ_c as a function of $\mathcal{N}$ in the logarithmic scale showing a linear dependency as $\ln(\Gamma_c) \approx A \ln(\mathcal{N}) + B$, where $A = -0.954$ and $B = 1.606$. This empirical relation allows us to determine the threshold value for the unbroken $\mathcal{PT}$ regime to excite the stable DS.

B. Discrete soliton and diffractive radiation

In absence of any $\mathcal{PT}$-symmetric potential ($\Gamma = 0$) the propagation equation becomes

$$i\frac{d\psi_n}{d\xi} + c[\psi_{n+1} + \psi_{n-1}] + |\psi_n|^2\psi_n = 0, \qquad (3)$$

which is the standard form of the DNLSE. In absence of non-linearity ($\gamma = 0$) Eq. (3) reduces to an analytically integrable equation whose solution $\psi_n(\xi) = \psi_n(0)i^n J_n(2c\xi)$ exhibits discrete diffraction. Now exploiting the discrete plane-wave solution $\psi_n(\xi) = \psi_0[i(nk_xd + \beta\xi)]$ of Eq. (3), one can obtain the standard dispersion relation between the longitudinal wave vector β and k_x as $\beta(\kappa) = 2c\cos(\kappa) + |\psi_0|^2$, where d is the separation between two adjacent waveguides, k_x is the transverse wave vector, and $\kappa \equiv k_x d$ is the dimensionless Bloch momentum defined as the phase difference between two adjacent waveguides [19]. The Taylor expansion of $\beta(\kappa)$ about the incident wave number (κ_0) results in the diffraction relation

$$\beta(\kappa) = \beta(\kappa_0) + \sum_{m\geqslant 1}\frac{D_m}{m!}\Delta\kappa^m, \qquad (4)$$

where $D_m \equiv (d^m\beta/d\kappa^m)|_{\kappa_0}$ and $\Delta\kappa = \kappa - \kappa_0$. The parameter D_1 represents the transverse velocity. Performing a Fourier transformation to change the domain as $\kappa \to n$ by replacing $\Delta\kappa \equiv -i\partial_n$, where n is defined as a continuous variable of an amplitude function $\Psi(n, \xi) = \psi_{n,\xi}\exp(-i\kappa_0 n)$, we obtain an approximate standard *nonlinear Schrödinger equation* (NLSE) [7]:

$$\left[i\partial_\xi + \sum_{m\geqslant 2}\frac{D_m}{m!}(-i\partial_n)^m + |\psi(n, \xi)|^2\right]\psi(n, \xi) = 0. \qquad (5)$$

One can eliminate the first and second term of the Taylor expansion by making a transformation $\psi(n, \xi) \to \psi(n, \xi)\exp[i\beta(\kappa_0)n]$ and considering the comoving frame

$n \to (n + D_1\xi)$. For $D_{m\geqslant 3} = 0$ one can have the exact solution of Eq. (5) as $\psi_{\mathrm{sol}} = \psi_0\mathrm{sech}(\frac{n\psi_0}{\sqrt{|D_2|}})\exp(ik_{\mathrm{sol}}\xi)$, where $k_{\mathrm{sol}} \equiv \psi_0^2/2$ is the longitudinal wave number of the soliton. Note that a bright soliton exists only when the condition $|\kappa_0| < \pi/2$ or $2c\cos(\kappa_0) > 0$ is satisfied. Figure 1(d) describes the formation of such soliton that propagates in a nonlinear uniform WA for an input beam $\psi_{\mathrm{sol}} = \psi_0\mathrm{sech}(n\psi_0/\sqrt{|D_2|})$. In Fig. 1(e) the spatial distribution of the DS is illustrated in the background of the periodic refractive index grid offered by the typical WA. Note, here the evolving soliton encompasses several waveguides, which justifies the continuous variable approximation of n. The plane-wave solution $\exp[i(k_{\mathrm{lin}}\xi + \Delta\kappa n)]$ of the linearized Eq. (5) leads to the dispersion relation $k_{\mathrm{lin}}(\Delta\kappa) = \beta(\kappa) - \beta(\kappa_0) - D_1\Delta\kappa$. A soliton with initial transverse wave number (κ_0) is described by

$$\psi_{\mathrm{sol}} = \psi_0\mathrm{sech}[n\psi_0/\sqrt{|D_2|}]\exp[i\kappa_0 n]. \qquad (6)$$

To solve the DNLSE [see Eq. (3)] numerically, we consider the input as Eq. (6), which is the solution of Eq. (5), the continuous form of NLSE. This soliton emits radiation in κ space by transferring energy to the linear wave when the condition $k_{\mathrm{sol}} = k_{\mathrm{lin}}(\Delta\kappa)$ is satisfied for a specific Δk. The phase-matching (PM) condition for generating DifRR [7] can be written as

$$[\cos(\kappa) - \cos(\kappa_0) + \sin(\kappa_0)\Delta\kappa] = \widetilde{\psi_0}^2 \qquad (7)$$

where $\widetilde{\psi_0} = \psi_0/2\sqrt{c}$. The solution of Eq. (7) gives the wave number of the generated DifRR ($\kappa_{\mathrm{RR}} = \kappa_0 + \Delta\kappa$) as a function of the initial soliton wave number κ_0 which is related to the incident angle of the beam.

In Fig. 2(a), formation of the DifRR in n space is demonstrated when the DS of amplitude $\psi_0 = 0.8$ is launched with an inclination of $\kappa_0 = 0.7$. The signature of DifRR (around -2.8) is prominent in κ space as illustrated in Fig. 2(b). In Fig. 2(c), we plot the spectrogram, which is mathematically defined as $\mathcal{S}(n, \kappa, \xi) = |\int_{-\infty}^{\infty}\psi(n', \xi)\psi_w(n - n')e^{i\kappa n'}dn'|^2$, where ψ_w is a reference window function (normally taken as input). This plotting scheme allows us to represent the output in n-κ space, where we clearly observe the formation of DifRR and DS. We calculate the spatial delay line $\delta_s = D_1\xi$ at output, which is analogous to the temporal delay usually calculated for the supercontinuum generation process in photonic crystal fibers. This delay line indicates the relative locations of different components (soliton and radiations) in n-κ space. Note, in the reduced scheme, the formation of DifRR is restricted within the first Brillouin zone ($\kappa_{\mathrm{RR}} < |\pi|$) and undergoes a shift (formally knows as *anomalous recoil*) in its wave number by $\pm 2\pi$ when they form outside these limits. In the top inset of Fig. 2(c), we plot the PM expression [Eq. (7)] whose solution predicts the Bloch momentum (κ_{RR}) of DifRR. The formation of DifRR is found to be sensitive to the relative values of κ_0 and ψ_0. In Fig. 2(d), we provide a phase plot in κ_0-ψ_0 space showing a forbidden region (gray region) for DifRR to generate. That means DifRRs are suppressed for the set of (κ_0, ψ_0) values falling on the gray region.
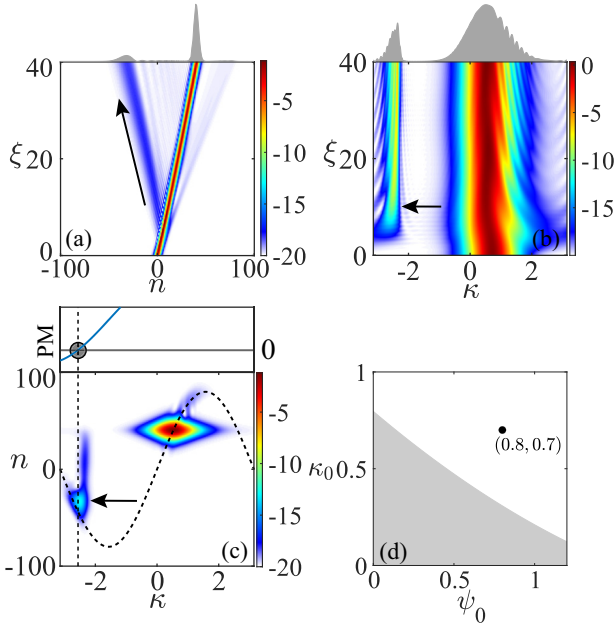
FIG. 2. (a) Formation of the weak linear wave corresponding to DifRR in n space when a tilted DS is launched. (b) A prominent signature of DifRR in κ space around the value $\kappa = -2.8$ and (c) the corresponding XFROG spectrogram at the output (marked by the arrow). The dotted line represents the spatial delay line defined as $\delta_s = D_1\xi$. In the inset, we plot the PM expression [Eq. (7)] whose solution predicts the Bloch momentum (κ_{RR}) of DifRR. (d) Phase plot showing the regime of (ψ_0, κ_0) values to generate the DifRR. The gray region is forbidden for DifRR to generate. The point indicates (ψ_0, κ_0) values in the phase plot for which the DifRR generation is shown in (a)–(c).

III. DIFFRACTIVE RADIATION IN A $\mathcal{PT}$-SYMMETRIC WAVEGUIDE ARRAY

In this section, we investigate the dynamics of a DS in a semi-infinite $\mathcal{PT}$-symmetric waveguide array with a neutral central waveguide. The schematic diagram of the WA is depicted in Fig. 1(a), where asymmetric gain-loss channels are arranged on either side of the central waveguide ($n = 0$). For a large number of waveguides ($\mathcal{N}$), the EP approximately obeys the relation $\ln(\Gamma_c) \approx A \ln(\mathcal{N}) + B$. For a linear $\mathcal{PT}$-symmetric WA with $\mathcal{N} = 501$, the EP reduces to as small as $\Gamma_c \approx 0.013$. In Fig. 3, we compare the dynamics of the DS for unbroken and broken symmetry regimes by taking two different Γ values. In Figs. 3(a)–3(c), we demonstrate the evolution of a DS launched at the neutral waveguide ($n = 0$) for $\Gamma = 0.01$ (which is in unbroken symmetry regime $\Gamma < \Gamma_c$). In this limit, we observe the propagation of a stable soliton which spreads over a few waveguide channels. The field is also localized in the Fourier domain [κ domain, see Fig. 3(b)]. The spectrogram in Fig. 3(c) clearly indicates the formation of a localized field at output. Dramatic change is observed when we increase the $\mathcal{PT}$ parameter to $\Gamma = 0.08$ ($> \Gamma_c$) which corresponds to the broken-symmetry regime. In this limit, the soliton which was initially extended to a few waveguides squeezes to a single waveguide (preferably the waveguide channel with gain) as shown in Fig. 3(d). This tight confinement of the soliton in the n domain results in an
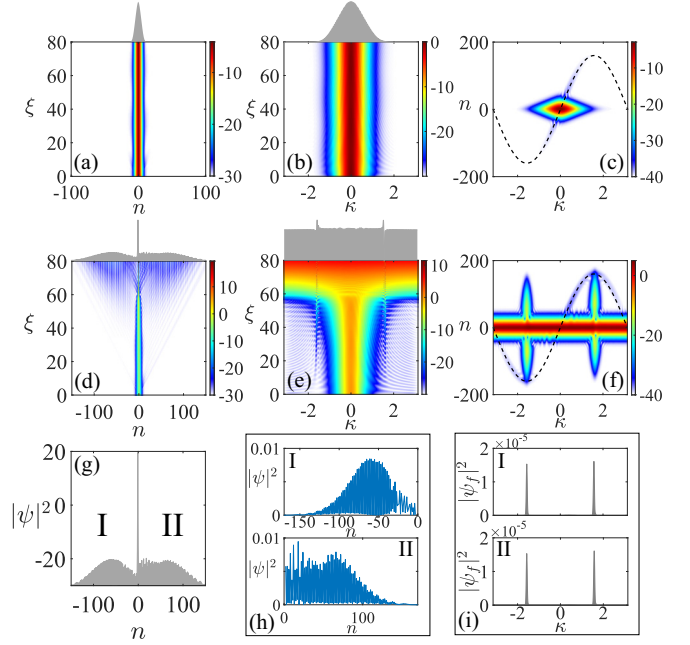

FIG. 3. Spatial soliton formation in (a) n space and (b) κ space with (c) spectrogram at the output $\xi = 80$. Here soliton amplitude $\psi_0 = 0.8$ and Γ of 0.01 ($< \Gamma_c$). Dynamics of DS in (d) n space and (e) κ space with (f) spectrogram at the output $\xi = 80$ for $\Gamma = 0.08$ ($> \Gamma_c$) in $\mathcal{PT}$-symmetry-breaking regime. (g) Tight confinement of soliton for Γ beyond EP exhibiting strong side lobes represented as I and II. (h) Individual representation of the side lobes (I, top; II, bottom) and (i) their Fourier transform showing radiations at $\kappa = \pm\pi/2$.

outburst in the Fourier space (κ domain) showing a continuous band [see Figs. 3(e) and 3(f)]. Side lobes are formed in n channels as the energy flows through the assistance of alternative gain channels of the WA. This field distribution of side lobes results in two peaks in the Fourier domain (κ space) at precise location $\pm\pi/2$ evident in Fig. 3(f). The side wings I and II in Fig. 3(g) independently contribute to the peaks. A Fourier transform of the two side lobes I and II [Fig. 3(h)] results in two distinct peaks at $\pm\pi/2$ [Fig. 3(i)]. These are the signature peaks for a $\mathcal{PT}$-symmetric waveguide array when a soliton is excited beyond the EP.

A. Dynamics of a strong DS (for $\kappa_0 \neq 0$) in a $\mathcal{PT}$-symmetric WA

In this subsection, we concentrate on the dynamics of a strong DS inside a $\mathcal{PT}$-symmetric WA and try to investigate the background mechanism of radiations emitted by this strong soliton. It is already demonstrated that DifRRs emerge over a threshold value of the pair (ψ_0, κ_0). Generally, for strong solitons (with high ψ_0) the formation of DifRR is evident. Here, a strong soliton ($\psi_0 = 0.6$) is launched with a phase gradient (nonzero κ_0 value) as shown in Fig. 4(a). This propagation dynamics leads to four distinct radiation peaks in κ space marked by ①–④ in Fig. 4(b). The radiation marked as ① is distinctly identified as DifRR. However, the origin of the other three radiations is solely due to the $\mathcal{PT}$-symmetric characteristics of WA because they are absent
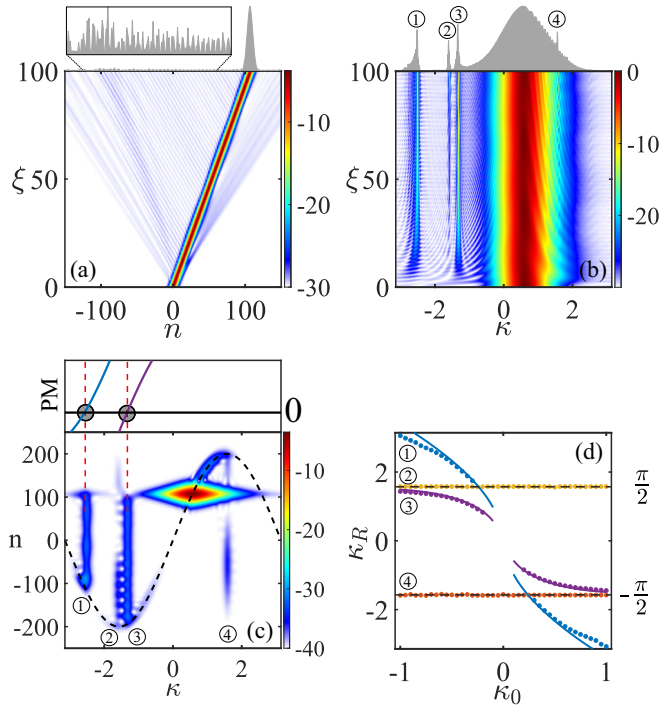
FIG. 4. (a) Soliton propagation with initial amplitude $\psi_0 = 0.6$ and wave number $\kappa_0 = 0.6$ for $\Gamma = 0.04$. In the inset, we magnify the localization of the $\mathcal{PT}$-symmetry-assisted pedestal field. (b) Emissions of different radiations in κ space marked as ①–④. (c) Spectrogram at the output. In the inset, we plot the phase-matching (PM) relation for both the standard DifRR ① and a $\mathcal{PT}$-symmetry-assisted radiation ③. (d) Variation of DifRR ① and $\mathcal{PT}$-symmetry-assisted radiation ③ as a function of κ_0, where numerical results (solid dots) are compared with proposed PM equations (solid lines). Radiations ② and ④ indicate the characteristic radiation at $\pm\pi/2$ (black dashed lines) independent of κ_0.

when the $\mathcal{PT}$ symmetry is switched off. Radiations ② and ④ represent the characteristic radiations at $\pm\pi/2$ generated due to the $\mathcal{PT}$-symmetry-assisted side-lobe propagation. It is worth noting that for a weak Γ value these radiations are suppressed. Therefore, in the simulation, we consider a value of Γ above the threshold EP value of the system such that soliton collapse does not happen up to a reasonable distance and at the same time the $\pm\pi/2$ radiations are prominent. In the inset of Fig. 4(a), we magnify the pedestal part of the moving soliton, showing how the side lobes are confined preferably in alternative gain channels, resulting in a periodic localized distribution in n space. A simple spatial Fourier transform of this periodic distribution of the pedestal field leads to the distinct radiation at $\pm\pi/2$ in κ space. Interestingly, in the Fourier space, we observe another radiation marked as ③ whose origin needs to be addressed. To understand the complete picture, we plot the spectrogram in Fig. 4(c), where all the radiations appear as stains in n-κ space over spatial delay line δ_s (dotted curve). It is observed that the radiations ③ and ② are closely spaced in κ space and spread over the n domain. Unlike ② and ④, the location of the radiation ③ is found to be sensitive to the initial launching angle (κ_0 value) of the DS. In Fig. 4(d), we track down all the radiations as a function of κ_0 ranging from -1 to $+1$. Note that for $|\kappa_0| < 0.25$ the radiations

① and ③ are suppressed. However, as expected, the characteristic radiations ② and ④ located at $\pm\pi/2$ remain unaffected by the variation of κ_0. While the phase-matching equation Eq. (7) (solid line) predicts the location of DifRR (radiation ①), the exact reason for the generation of radiation ③ is still unknown.

Pertaining to the origin of radiation ③, in our system, we consider a WA with an alternative gain-loss arrangement having a neutral waveguide channel at the center ($n = 0$). We obtain the dispersion relation for this system by analyzing the array as a diatomic lattice or two-level system [23], $\beta_{\mathcal{PT}}(\kappa) = \sqrt{4c^2 \cos^2 \kappa - \Gamma^2}$, where the edge of the Brillouin zone is defined at $\kappa = \pm\pi/2$. Adopting the PM condition similar to Eq. (7), we can expect a $\mathcal{PT}$-symmetry-assisted radiation when

$$\beta_{\mathcal{PT}}(\kappa) - \beta_{\mathcal{PT}}(\kappa_0) - D_1 \Delta\kappa = \psi_0^2/2, \tag{8}$$

where $D_1 = \partial_\kappa \beta_{\mathcal{PT}}(\kappa)|_{\kappa=\kappa_0}$. The solutions to Eq. (8) are subjected to the boundary condition $|\kappa| = \pi/2$ due to the resulting Brillouin zone where a shift of $\pm\pi$ in the wave number is required for anomalous recoiling. The proposed PM relation Eq. (8) accurately predicts the $\mathcal{PT}$-symmetry-assisted resonant radiation in κ space as demonstrated in Fig. 4(c). We generalize the theory for a range of κ_0 (violet solid lines) and find an excellent agreement with full numerical results (violet solid dots) as shown in Fig. 4(d).

B. Dynamics of a weak DS (for $\kappa_0 \neq 0$) in a $\mathcal{PT}$-symmetric WA

In this subsection, we investigate the dynamics of a weak soliton inside a $\mathcal{PT}$-symmetric WA. Here we mainly show how the radiations emitted by a weak soliton are characteristically different from the radiation emitted by a strong DS. Based on the phase plot [see Fig. 2(d) in Sec. II B], the soliton parameters are chosen in such a way that both DifRR and $\mathcal{PT}$-symmetry-assisted radiations are suppressed. Note, the spatial width of the DS is inversely proportional to its amplitude, and hence, a weak soliton encompasses a large number of waveguide channels and also experience a smaller amount of *Peierls-Nabarro* potential [24] during transverse propagation. This increases the interaction possibility of the soliton with periodic gain-loss channels. To understand the interaction between a weak soliton and defect, we first consider a uniform WA having a gain-loss channel (or a coupler) located at sites $n = 30, 31$. This coupler embedded within the uniform neutral WA should act as a defect center for light scattering. In Fig. 5(a), we demonstrate the propagation of the weak DS, which experiences the defect created by the pair of $\mathcal{PT}$-symmetric gain-loss channels. Note that due to the low amplitude and initial momentum, the DS does not produce the regular DifRR in κ space; the only radiation it produces is due to the reflection from the defect boundary, which is evident in Fig. 5(b). The spectrogram plot in Fig. 5(c) showcases the formation of radiation (highlighted by an arrow) due to the scattering from the defect boundary. A simple momentum conservation predicts the location of this radiation in κ space as $\kappa_R = -\kappa_0$ and demonstrated in Fig. 5(d) where solid dots represent the κ_R value obtained numerically. Note that, as expected, in this system the characteristic $\pm\pi/2$ side lobes are absent due to the absence of $\mathcal{PT}$-symmetric periodicity.
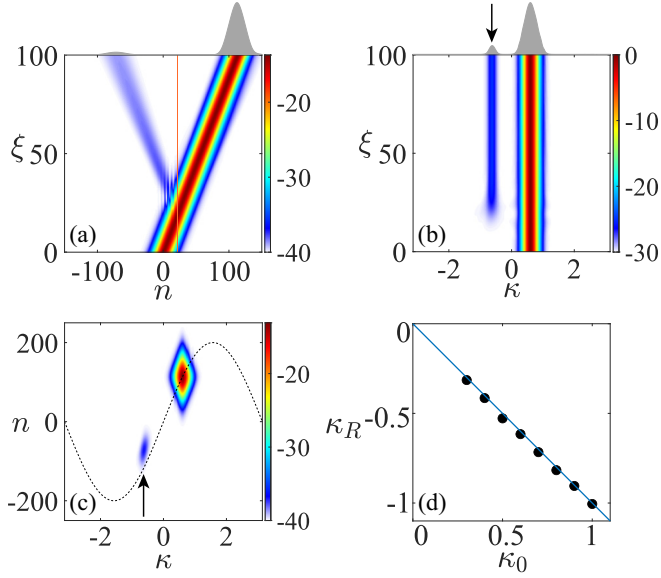
FIG. 5. Interaction of a low amplitude soliton of ($\psi_0 = 0.2$) with a single $\mathcal{PT}$-symmetric element. (a) Soliton movement in n space where a low amplitude reflection takes place from the defect boundary. (b) The reflected component emerges as a radiation at $\kappa = -\kappa_0 = 0.6$ in the κ domain. (c) The spectrogram at the output shows that both the soliton and reflected components follow the delay line. (d) Locations of the reflected component in κ space obtained numerically (solid dots) for different initial κ_0. The numerical results are consistent with the reflection condition of $\kappa = -\kappa_0$ shown by the solid blue line.

In our original setup of the $\mathcal{PT}$-symmetric WA, the gain-loss channels are arranged alternatively with a neutral channel placed at the center ($n = 0$) that acts as a defect. When we extend our investigation in such a system for a weak DS, a few more interesting aspects emerge which were obscured in the dynamics of a strong soliton. Here the weak soliton ($\psi_0 = 0.2$) with initial phase gradient radiates four distinct radiations [see Figs. 6(a) and 6(b)]. Radiation ⑥ can be identified as the reflection from the central defect in the $\mathcal{PT}$-symmetric WA, similar to what we have observed in Fig. 5 as it follows the same $\kappa_R = -\kappa_0$ relationship. The localization of the fields ② and ④ at $\pm\pi/2$ in κ space is also observed for the weak DS. However, the formation of the radiation ⑤ is surprising and one can confuse it with the DifRR. Radiation ⑤ must be different from DifRR since the formation of DifRR is suppressed for the given parameters of the soliton. We observe that a forward propagating weak soliton (which covers more waveguide channels) experiences a significant backscattering due to the periodic $\mathcal{PT}$-symmetric elements and produces an additional radiation (in κ space). Notably, the radiation ⑤ originates almost from $\xi = 0$ point which supports the backscattering theory. In the spectrogram plot [Fig. 6(c)] also the signature of backscattering ⑤ is evident as it is located at the same spatial location (n coordinate) as that of the soliton but on the reverse delay curve. The phase of the backscattered wave is detuned by π and under the folded Brillouin zone scheme one can calculate its momentum as $\kappa_{BS} = (\kappa_0 - \pi)$. In Fig. 6(d), we plot the momentum of all four radiations (including ⑤) as a function of input soliton wave number κ_0
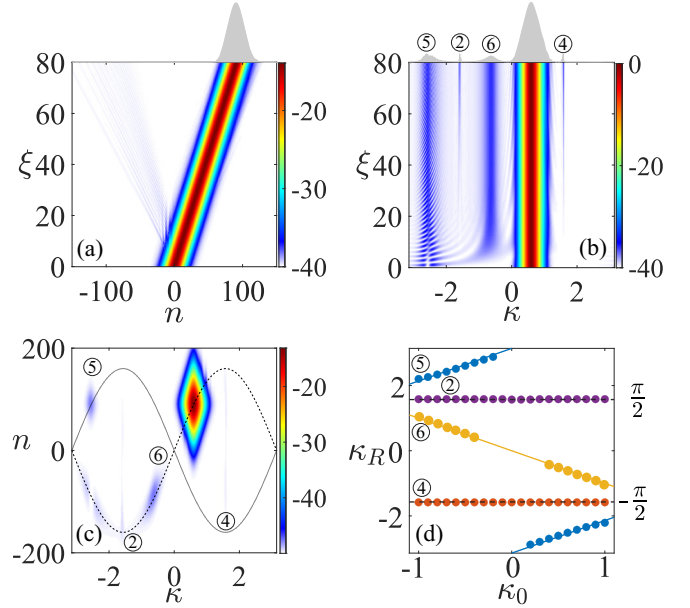

FIG. 6. (a) Propagation of a low amplitude ($\psi_0 = 0.2$, $\kappa_0 = 0.6$) soliton in a $\mathcal{PT}$-symmetric WA with where DifRR is suppressed. (b) Different radiations on κ space marked as ②, ④, ⑤, and ⑥. (c) Spectrogram at output with delay curves. (d) Variation of different radiations as a function of κ_0. The solid dots are numerical results, whereas the lines correspond to the theory.

and find a satisfactory matching between simulation data with the theory that we proposed.

IV. CONCLUSIONS

In this paper, we explain the origin of a few unique radiations that take place when a discrete soliton is excited inside a $\mathcal{PT}$-symmetric waveguide array. The concept of $\mathcal{PT}$ symmetry is optically realized by constructing a waveguide array with alternative gain-loss channels. We perform a linear Hamiltonian analysis to obtain the operational regime in a $\mathcal{PT}$-symmetric system. The dynamics of a spatial soliton are investigated under such a system where several distinctive radiations emerge in the momentum space due to the $\mathcal{PT}$ symmetry. A strong discrete soliton when launched with an inclination emits diffractive resonance radiation. The $\mathcal{PT}$-symmetric nature of the waveguide array, however, excites several other radiations that have not been explored. We make an attempt to investigate the physical origin of all these radiations and put forward a background theory. It is found that under the limit of broken $\mathcal{PT}$ symmetry when the optical field is launched normally to the central neutral channel, it squeezes to the adjacent gain waveguide with a pedestal extending over n space. This leads to the population of the field at $\pm\pi/2$ in momentum space (κ space) and is identified as characteristic radiation of a $\mathcal{PT}$-symmetric waveguide array. Distinctive $\mathcal{PT}$-symmetry-assisted radiation also emerges for a strong soliton due to the diatomic arrangement of lattices. We establish a modified phase-matching relation that predicts the location of this radiation in momentum space. A weak soliton also emits a few distinct radiations which are

characteristically different. For example, a weak tilted soliton interacts with the central defect in the $\mathcal{PT}$-symmetric WA resulting in a radiation in the form of reflection. In such systems, a backscattering is also observed which is prominent for a weak soliton propagating through a full $\mathcal{PT}$-symmetric system and leads to a different kind of radiation. We characterized all these radiations and established a background theory which is found to be in good agreement with full numerical simulation. Our results might be useful for next generation light shaping and optical switching applications.

ACKNOWLEDGMENT

[1] Y. Lahini, A. Avidan, F. Pozzi, M. Sorel, R. Morandotti, D. N. Christodoulides, and Y. Silberberg, Phys. Rev. Lett. **100**, 013906 (2008).

[2] L. Martin, G. D. Giuseppe, A. Perez-Leija, R. Keil, F. Dreisow, M. Heinrich, S. Nolte, A. Szameit, A. F. Abouraddy, D. N. Christodoulides, and B. E. A. Saleh, Opt. Express **19**, 13636 (2011).

[3] R. Morandotti, U. Peschel, J. S. Aitchison, H. S. Eisenberg, and Y. Silberberg, Phys. Rev. Lett. **83**, 4756 (1999).

[4] T. Pertsch, P. Dannberg, W. Elflein, A. Bräuer, and F. Lederer, Phys. Rev. Lett. **83**, 4752 (1999).

[5] B. M. Breid, D. Witthaut, and H. J. Korsch, New J. Phys. **8**, 110 (2006).

[6] F. Dreisow, A. Szameit, M. Heinrich, T. Pertsch, S. Nolte, A. Tünnermann, and S. Longhi, Phys. Rev. Lett. **102**, 076802 (2009).

[7] T. X. Tran and F. Biancalana, Phys. Rev. Lett. **110**, 113903 (2013).

[8] T. X. Tran, D. C. Duong, and F. Biancalana, Phys. Rev. A **89**, 013826 (2014).

[9] D. V. Skryabin and A. V. Gorbach, Rev. Mod. Phys. **82**, 1287 (2010).

[10] A. P. Lara and S. Roy, Phys. Rev. A **102**, 033512 (2020).

[11] C. M. Bender and S. Boettcher, Phys. Rev. Lett. **80**, 5243 (1998).

[12] M.-A. Miri and A. Alù, Science **363**, eaar7709 (2019).

[13] R. El-Ganainy, K. G. Makris, M. Khajavikhan, Z. H. Musslimani, S. Rotter, and D. N. Christodoulides, Nat. Phys. **14**, 11 (2018).

[14] B. Peng, Ş. K. Özdemir, F. Lei, F. Monifi, M. Gianfreda, G. L. Long, S. Fan, F. Nori, C. M. Bender, and L. Yang, Nat. Phys. **10**, 394 (2014).

[15] A. Guo, G. J. Salamo, D. Duchesne, R. Morandotti, M. Volatier-Ravat, V. Aimez, G. A. Siviloglou, and D. N. Christodoulides, Phys. Rev. Lett. **103**, 093902 (2009).

[16] M. Wimmer, A. Regensburger, M.-A. Miri, C. Bersch, D. N. Christodoulides, and U. Peschel, Nat. Commun. **6**, 7782 (2015).

[17] J. Wiersig, Phys. Rev. Lett. **112**, 203901 (2014).

[18] H. Hodaei, A. U. Hassan, S. Wittek, H. Garcia-Gracia, R. El-Ganainy, D. N. Christodoulides, and M. Khajavikhan, Nature (London) **548**, 187 (2017).

[19] D. N. Christodoulides and R. I. Joseph, Opt. Lett. **13**, 794 (1988).

[20] Y. V. Kartashov and V. A. Vysloukh, Opt. Lett. **44**, 791 (2019).

[21] B. Zhu, H. Zhong, J. Jia, F. Ye, and L. Fu, Phys. Rev. A **102**, 053510 (2020).

[22] A. Sahoo and A. K. Sarma, Phys. Rev. A **106**, 023508 (2022).

[23] Y.-L. Xu, W. S. Fegadolli, L. Gan, M.-H. Lu, X.-P. Liu, Z.-Y. Li, A. Scherer, and Y.-F. Chen, Nat. Commun. **7**, 11319 (2016).

[24] W. Królikowski and Y. S. Kivshar, J. Opt. Soc. Am. B **13**, 876 (1996).